Analysis of Medium-Speed Runway Exit Manoeuvres

Etienne Coetzee *
Systems General, Airbus, Bristol, UK, BS99 7AR
Bernd Krauskopf† and Mark Lowenberg‡
Faculty of Engineering, University of Bristol, Bristol, UK, BS8 1TR

Recent studies suggest that fuel savings can be realised if more efficient surface movements can be achieved through means other than the engines of an aircraft, or by optimising the scheduling of aircraft on the ground. All aspects of ground manoeuvring therefore need to be studied to understand the impact of such changes. This paper presents an analysis method for medium-speed manoeuvres, and, more specifically, runway exit manoeuvres. Kinematic equations that were derived for towing analysis form the basis of the runway exit study, from which empirical formulas are derived for steering angle and clearance predictions. The results of the empirical method compare very well with kinematic studies, as well as detailed dynamic model simulations, as is demonstrated with the test case example of an A380 model. The empirical formulas can be used to great effect during the early design phases of an aircraft programme for the prediction of steering angles and clearance distances, when very little data is available. The greatest advantage of the proposed method is that any aircraft configuration or runway exit can be analysed.

Nomenclature

C	=	position vector of reference point mid way between the main gears, relative to an inertial coordinate system (-)
c_x	=	x-position of reference point mid way between the main gears, relative to an inertial coordinate system (-)
c_y	=	y-position of reference point mid way between the main gears, relative to an inertial coordinate system (-)
CG	=	Centre of Gravity
COC	=	Cockpit Over Centreline
F	=	position vector of nose gear relative to reference point mid way between the main gears (-)
FAA	=	Federal Aviation Administration
FOD	=	Foreign Object Damage
$ICAO$	=	International Civil Aviation Organization
JOS	=	Judgemental Oversteer

*Systems Engineering Specialist.
†Professor, Department of Engineering Mathematics.
‡Senior Lecturer, Department of Aerospace Engineering. Senior Member AIAA.

l_{cm} = distance from CG to main gears reference position (m)
l_{cn} = distance from CG to nose gear (m)
L_m = track width normalised to wheel base (-)
l_m = track width: distance between outermost wheels of left and right outer gears, measured from outer wheel-plane (m)
l_n = wheelbase: distance from nose gear to main gears reference position (m)
M = position vector of inner main gear reference position, relative to an inertial coordinate system (-)
m = mass (kg)
m_x = x-position of reference point of inner main gears during a turn, relative to an inertial coordinate system (-)
m_y = y-position of reference point of inner main gears during a turn, relative to an inertial coordinate system (-)
N = position vector of nose gear, relative to an inertial coordinate system (-)
n_x = x-position of nose gear, relative to an inertial coordinate system (-)
n_y = y-position of nose gear, relative to an inertial coordinate system (-)
R_m = radius of turn measured from the turn-centre to outer wheel-plane of innermost gear during turn, normalised to wheelbase (-)
r_m = radius of turn measured from the turn-centre to outer wheel-plane of innermost gear during turn (m)
R_n = radius of turn measured from the turn-centre to the bottom of the nose gear strut, normalised to the wheelbase (-)
r_n = radial position of nose gear from turn-centre (m)
t = time (s)
V_n = magnitude of velocity at nose gear, measured in SI units (m/s) or normalised to wheelbase (1/s)
$\dot{V}_n$ = magnitude of acceleration at nose gear ($1/s^2$)
α_m = slip-angle at main tyre position (deg)
α_n = slip-angle at nose tyre position (deg)
δ = steering angle (deg)
δ_f = steady-state steering angle for a circle with a specific radius (deg)
δ_{90} = steering angle when nose gear reaches exit point for 90° turn (deg)
δ_{135} = steering angle when nose gear reaches exit point for 135° turn (deg)
θ_n = angular component of polar coordinate of nose gear position during a turn, measured from negative inertial x-axis (deg)
$\dot{\theta}_n$ = angular velocity of polar coordinate of nose gear position during a turn, measured from negative inertial x-axis (deg/s)
θ_m = angular component of polar coordinate of inner main gear reference position during a turn, measured from negative inertial x-axis (deg)
ψ = heading angle (or yaw angle), where north represents reference orientation (deg)

I. Introduction

Aircraft manufacturers are constantly striving to improve the efficiency of all aspects surrounding the operation of their aircraft. Obvious fuel savings can be made by decreasing the drag of the aircraft during the cruise phase. However, less obvious savings can be made by improving the way aircraft are operated on the ground. Recent studies seem to indicate that efficiencies can be made if surface movements can be achieved through means other than that of the engines [1]. A large amount of fuel is consumed when an aircraft's main engines are used to taxi around airports, where a forecasted total cost of fuel consumption during taxiing of around $7bn annually, is predicted by 2012 [1]. It is also predicted that this type of fuel consumption leads

to CO_2 emissions of approximately 18m tonnes per year, while Foreign Object Damage (FOD) contributes to a cost of around $350m per year [1]. New operational procedures are also directed towards the reduction of noise, and taxiing consequently impacts the environment in terms of air and noise pollution. Several schemes for saving fuel on the ground have been proposed. The Taxibot [1] project is one such scheme, where the engines are shut down and the pilot controls the movement of the aircraft on the ground via a remotely controlled tug. The Advisory Council for Aeronautics Research in Europe proposes a method where automation of ground manoeuvres, and optimal scheduling, can contribute towards fuel reductions [2]. This proposed drive towards alternative means for ground manoeuvres implies that all aspects of ground manoeuvres need to be understood for all possible speed ranges.

We start the paper in section II by discussing the types of ground manoeuvres that are of importance, where we propose a scheme where ground manoeuvres are categorised according to the operational velocities of the aircraft. To this end, we define a low-speed (0-6 knots), medium-speed (6-14 knots) and high-speed ($>$ 14 knots) category, where figure 1 indicates the types of ground manoeuvres that can be conducted within each speed range. Only the shaded pieces are manoeuvres that are considered in this paper. The piece in the upper left-hand corner pertaining to U-turn manoeuvres was covered in [3]. The kinematic equations that were originally derived for low-speed towing manoeuvres of vehicles with trailers [4], an arrangement similar to an aircraft being towed, form the basis for the analysis of the medium-speed cases discussed in this paper. Future studies will focus on low and medium-speed towing, as well as the stability of an aircraft during high-speed ground manoeuvres, with the aim of filling out the bottom and right-hand side of the puzzle in figure 1.

There is a tendency nowadays to immediately resort to detailed simulation models whenever ground performance studies are conducted, even for tasks that could be performed by more efficient methods. This is mainly due to a perception that accurate performance predictions cannot be made unless detailed tyre and landing gear models are available. The art however lies in the use of the appropriate method, best-suited to the type of analysis under consideration. In this paper we propose a hierarchy of methods that can be used at various stages of an aircraft programme, where each method is rated for its suitability at the stage under consideration. The ultimate aim is to provide tools that can be used by design engineers at all stages of an aircraft programme, with an increasing level of complexity as the programme progresses. Steering angles and clearance distances are of importance during the preliminary design phase, while tyre forces and gear loads become more relevant during the detailed design phase. Figure 2 contains typical design phases during an aircraft programme, with the associated ground manoeuvring information that is required at each phase.

In section III we discuss the challenges related to multibody simulations, especially their computational cost. We then highlight the different methods that can be used for efficiency improvements, eventually focussing on alternative analysis methods. The first analysis method is a kinematic method that was originally developed for jackknifing studies [4]; it is suitable for clearance and steering angle investigations. The results from the kinematic method are used for the derivation of empirical formulas; it can be used to obtain accurate predictions for clearance distances and steering angles. The second method is based on bifurcation theory, more specifically continuation methods; it can be used to obtain turn-radii, or steady-state forces on any gear or tyre. This approach was used for the prediction of U-turn manoeuvres [5]. The final method makes use of simulations.

A validated dynamic simulation model of the Airbus A380 is used as a baseline for the study. The model is of considerable complexity, as it describes a large aircraft with 5 landing gears and 22 wheels. It contains all aspects that are of importance to the dynamics of the aircraft on the ground, including the tyre properties, gear flexibility, brake logic, engine properties, tow configurations, and different mass configurations. This model provides a versatile means of investigating different configurations and propulsion schemes for towing and exit manoeuvres [3]. The different methods are compared for the A380 baseline model, and a judgement is made with regards to the suitability of each method for the analysis of medium-speed ground manoeuvres.

The strength of the approach presented is its suitability for *any aircraft or runway configuration*. Table 1 contains a summary of the applicability of the methods discussed in this paper, to the types of questions a design engineer might ask when medium-speed ground manoeuvres are considered. The reference to stability refers to an appropriate measure of stability and its change when a parameter is varied (such as root locus plots), and not merely to observations from simulations. It is usually not a trivial process to obtain root locus information from multibody simulations, hence the reason for omitting this capability in table 1. Design of Experiments is also used with simulations to try and build a map of the dynamics, however, the method is computationally expensive with no guarantee that all the dynamics have been categorised.

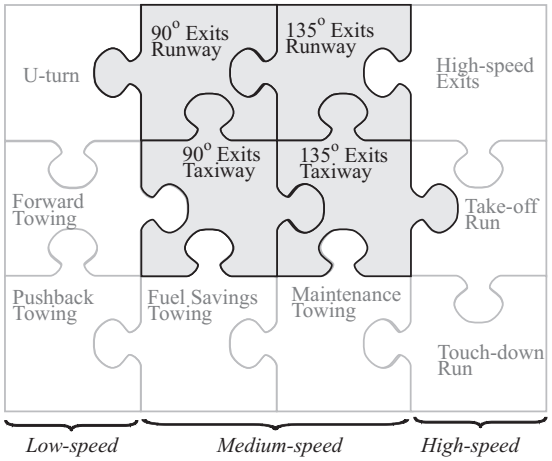

Figure 1: Types of ground manoeuvres. Shaded pieces indicate areas of interest for this paper, while faded pieces are the topics of past and future research.

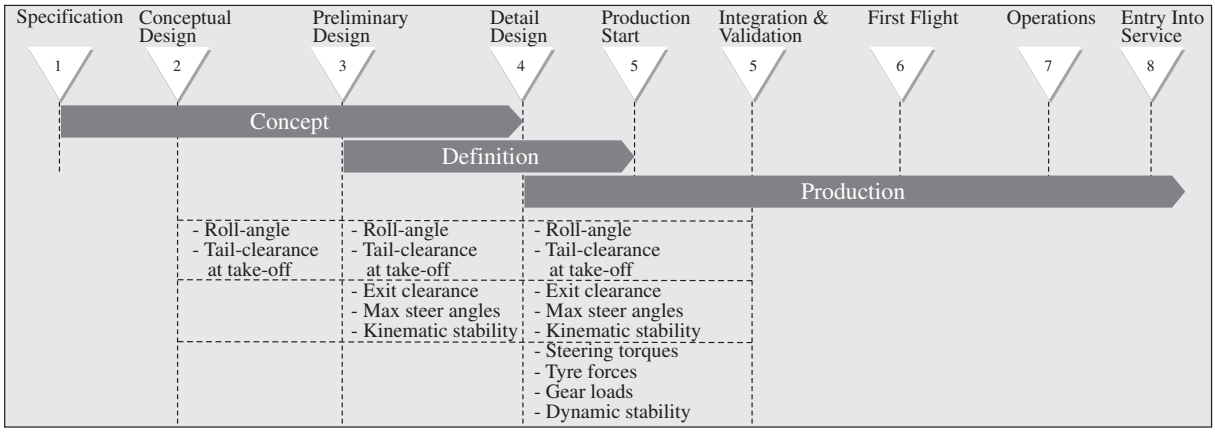

Figure 2: Design phases with typical ground manoeuvring requirements for each phase.

In section IV we show that an exit manoeuvre is essentially a transition from a straight line to a circular trajectory, where the shape of the steering angle curve forms an exponential function, that eventually settles into a steady-state value. This is contrary to previous approaches where a ramp input is assumed [6]. The kinematic method is used for the initial analysis of runway exit manoeuvres; it is however still deemed to be a difficult method for everyday use. Therefore empirical formulas for the steering angle variation that are derived, are valid *for any aircraft configuration*. A comparison is made between the empirical, kinematic, and dynamic methods, where we conclude that the empirical and kinematic methods are sufficient to predict the steering angle variation for a towed case, while a minor adjustment is needed for the self-propelled case. This adjustment is due to the nature of the constraint force that is needed to follow the centre line. The constraint force at the nose landing gear is provided by the tug in the towing case, and by the nose gear tyres in the case where the aircraft moves under its own power.

Empirical equations are derived in section V for the minimum clearance distances that can be expected for 90° and 135° exits, which are applicable to an aircraft that is being towed, or an aircraft that conducts a turn under its own power. We show that the clearance distances that are obtained for towing and self-propelled motion are the same, which is due to the dominant effect of the geometry and, more specifically, the wheelbase and track width. A comparison is again made between the empirical, kinematic, and dynamic methods, where it is shown that the error in the minimum clearance position for the empirical and kinematic solutions is within 1.5% of the dynamic simulation results. A diagram that indicates the feasibility of exit manoeuvres at Group V and VI airports is then constructed *for any aircraft configuration*; it gives valuable insight into the effects of wheelbase and track width on the clearance distances for specific configurations. This diagram can be used as an effective tool for design purposes.

Table 1: Applicability of methods for ground manoeuvre studies

	Empirical methods	Kinematic simulations	Bifurcation methods	Dynamic simulations
Clearance distances	✓	✓	×	✓
Steering angles	✓	✓	✓	✓
Forces	×	×	✓	✓
Kinematic stability	×	×	✓	×
Dynamic stability	×	×	✓	×
Ease of use	✓	✓	×	×
Computational efficiency	✓	✓	✓	×

II. Medium-speed Exit Manoeuvres

Aircraft ground operations are comprised of a combination of tug and self-propelled movements. Tug operations tend to consist of pushbacks from the gate until the aircraft reaches a favourable orientation for movement under its own power, or maintenance towing between hangars. Taxi operations, on the other-hand, are presently conducted with the aid of the aircraft's engines. One only has to venture to the nearest airport to notice that aircraft often stand around for extended periods while waiting for take-off clearance, which leads to unnecessary fuel consumption. Ideas related to the towing of aircraft to a starting grid close to the runway threshold have been mentioned for the purposes of fuel savings [1]. The movements of aircraft at runway exits under towed and self-propelled conditions are therefore of interest. This paper will focus on the self-propelled case, while a future study will focus on towing. A great deal of variance may exist in the way that any of the ground manoeuvres is conducted, whether around the apron or during taxiing. This is due to the nonlinear nature of the landing gears [3], as well as the variance of the inputs from the pilot. A good example that highlights this variance can be found in the A380 Airplane Characteristics Manual [7], which states:

> *"In the ground operating mode, varying airline practices may demand that more conservative turning procedures be adopted to avoid excessive tire wear and reduce possible maintenance problems. Airline operating techniques will vary in the level of performance, over a wide range of operating circumstances throughout the world. Variations from standard aircraft operating patterns may be necessary to satisfy physical constraints within the maneuvering area, such as adverse grades, limited area or high risk of jet blast damage. For these reasons, ground maneuvering requirements should be coordinated with the using airlines prior to layout planning".*

A main assumption in the present study is that the nose landing gear follows the taxiway centreline perfectly, with very little variance to either side. This is not neccessarily in line with the above quotation, but it does allow us to make a direct comparison of the methods under consideration. Future studies could focus on the sensitivity of exit manoeuvre trajectories to the variance in design parameters, and they can build on those conducted in reference [6]. Realistic ground manoeuvres reflect the typical scenarios that a pilot encounters during normal day-to-day operations. Two methods are used when conducting an exit manoeuvre. The judgemental oversteer (JOS) method is used where the pilot allows the nose gear to overshoot the centreline, so that the geometric mean point of the main gears follows the centreline. The JOS method is used on smaller taxiways where clearance distances are of concern, as is depicted in figure 3(a). The cockpit over centreline (COC) method is where the pilot steers the aircraft in such a way that the cockpit follows the centreline; it is depicted in figure 3(b). Symmetric thrust and brake inputs are used for these manoeuvres. Note that the outer engines are typically set to idle-thrust on very large 4-engined aircraft (such as the A380), for the avoidance of FOD. Design engineers would like to obtain an early view of what clearances and steering angles are needed to manoeuvre around specific airports. Very little design data is available at the concept phase of a project, yet the design engineer needs to make a decision on what the wheelbase and track width of the aircraft should be. These parameters affect the steering angles and clearances that will be obtained.

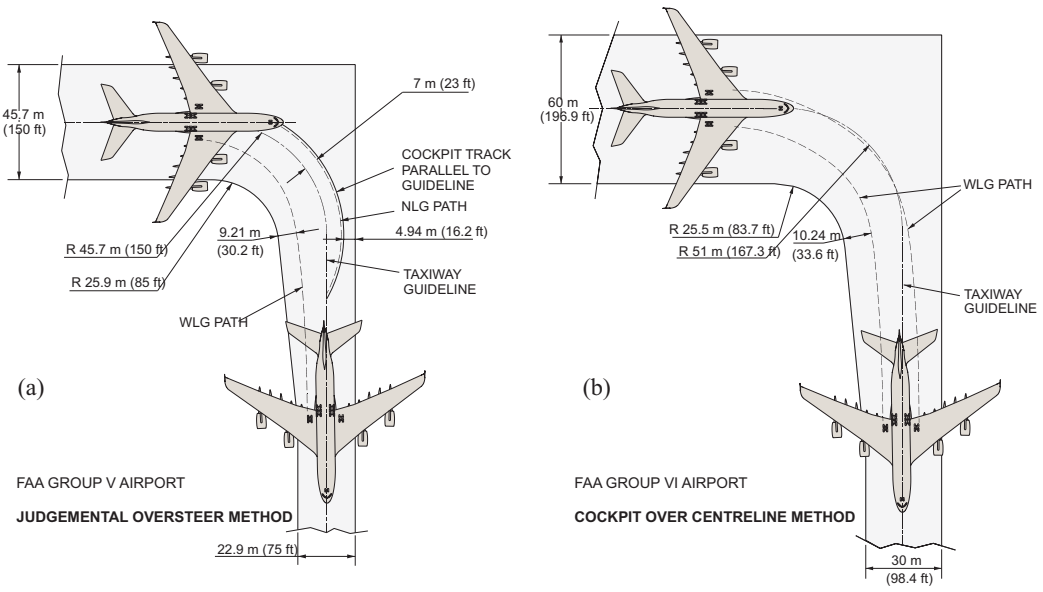

Figure 3: Extracts from the Airplane Characteristics Manual for the A380, showing the different methods for exiting the runway, based on the runway category [7]. (a) JOS method, (b) COC method.

Figure 4(a) depicts some relevant parameters for a runway exit, where an exit to the right is standard convention. The position of the nose gear on the centreline is depicted by the polar coordinates R_n and θ_n, and is measured in a clockwise direction from the negative x-axis. The heading (or yaw) angle is denoted by ψ. Figure 4(b) shows a simulation where the trajectories of specific points on the aircraft are traced out, of which the inner gear reference position is the most important for clearance purposes. The dashed circle represents the steady-state radius of the inner-gear reference position, which is for a scenario where the nose gear follows a circular trajectory equivalent to the radius of the exit. The aircraft will transition from a straight line trajectory onto a circular trajectory, eventually settling into a steady-state. It is important to note that the turn-centre is only located at the geometric centre of the circular arc when a steady-state is reached.

III. Hierarchy of Analysis Methods

Modelling and simulation forms an integral part of the design process. It is used for detailed performance predictions to test aircraft manoeuvrability under normal and abnormal conditions, as well as the definition of towing procedures for operators. Detailed models that contain all the physical characteristics of the gears and tyres are used to analyse the dynamics of an aircraft on the ground. The simulations are used to obtain clearance distances, steering angles, forces on the tyres and gears, and many other parameters of interest. However, there are drawbacks related to the run-times of dynamic simulations, the skills that are needed by specialist engineers to build satisfactory models, as well as the availability of data during the early design phases. The costs related to dynamic simulations make it necessary to evaluate the options that are available for the specific problem at hand. If the aim is to reduce the analysis time for a specific technical challenge, the following approaches can be followed:

- **Reduction of computational run-times**. This can either be achieved by using more powerful computational resources, or by focussing on more efficient algorithms. Recent work on the reformulation of the equations of motion by Udwadia and Kalaba [8] promises to ease the construction of the underlying equations, as well as provide improvements in the run-times.
- **Adapting the existing analysis method**. This refers to the use of existing models in a different way, specifically with bifurcation methods. A previous study [3] showed that steady-state solutions are sufficient to obtain accurate predictions for the turn-width that can be achieved during a U-turn manoeuvre. This method also incorporates accurate slip-angle and force data for the tyres.

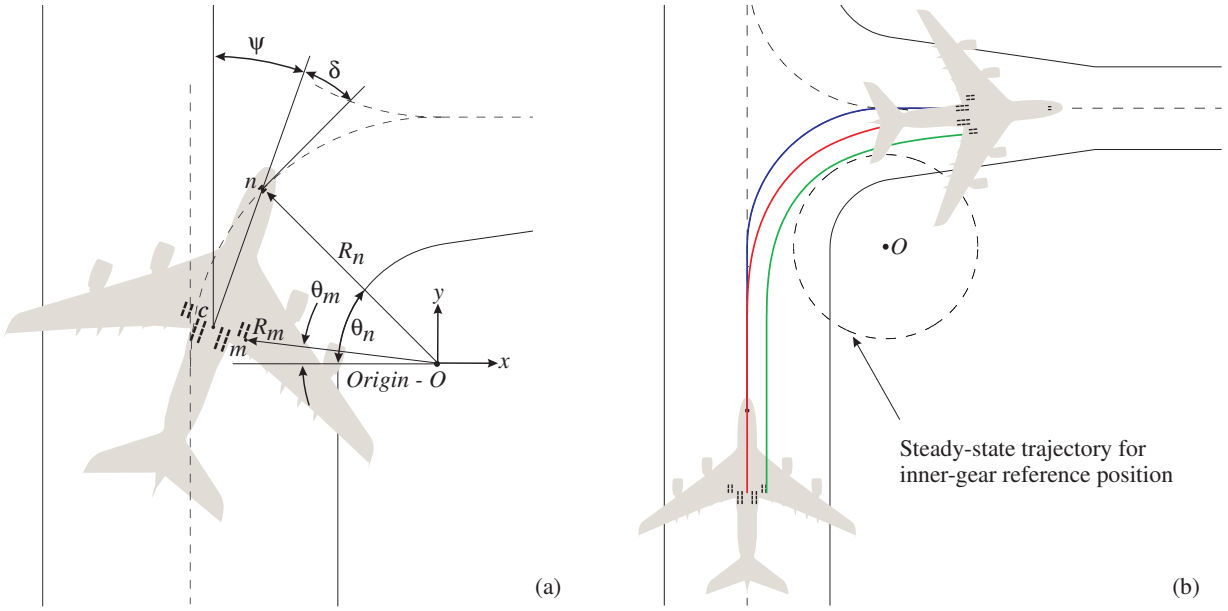

Figure 4: Relevant parameters for a 90° exit.

- **Using different analysis methods**. Simulations are not always needed, but have become popular due to the large amounts of information they are providing. Simulation should not be considered as a first option unless other options have been considered. An example would be the use of "lookup tables" for the calculation of tyre forces, instead of detailed tyre models.

Modelling is often seen as an art due to the nuances of certain aspects related to numerical accuracy, discontinuities, etc. Detailed modelling skills are often not needed where rules-of-thumb would suffice. Alternative methods should therefore be explored that can be used to formalize such rules-of-thumb, providing enough accuracy to serve as a valuable design tool, particularly when the detailed data that is needed for dynamic simulations is not yet available. Section III.A will focus on the use of kinematic analysis methods to characterise certain manoeuvres, as an alternative to dynamic simulations, while section III.B discusses the use of continuation methods to calculate turn-radii, tyre and gear forces. Finally, section III.C describes how dynamic models are built and used; the computational difficulties surrounding such dynamic simulations are also discussed. Kinematic analysis and continuation methods are thus presented as alternative means for steering angle and clearance predictions.

III.A. Kinematic Methods

A kinematic model describes only how points on a body move in relation to one another due to certain geometric constraints. It can therefore be used to study the motion of a body, while disregarding the forces that cause the motion. Dynamic analysis, on the other hand, incorporates these forces. A previous towing study by Fossum *et.al* [4] derived a kinematic model for the analysis of a truck with a trailer and classified the stability of the truck-trailer combination for straight-line and circular manoeuvres. The dimensions were normalised relative to the wheelbase $|l_n| = 1$.

The same equations can be used for an aircraft that conducts a runway exit manoeuvre under its own power, where the nose landing gear is constrained to follow a specific trajectory. This constraint is usually defined in the form of a velocity vector. Figure 5 represents the aircraft with a velocity vector defined at the nose gear. The main assumption is that the velocity vector at point c is along the longitudinal axis of the aircraft, where point c represents the mean position of all the bogie pivot points of the main gears. This assumption was shown in [4] to be sufficient, and it correlates with our own observations of the manoeuvres under consideration. The equations describing the velocity at point c are described by [4]:

$$\dot{C} = [\dot{N} \cdot (N - C)](N - C) \quad (1/\text{s}). \tag{1}$$

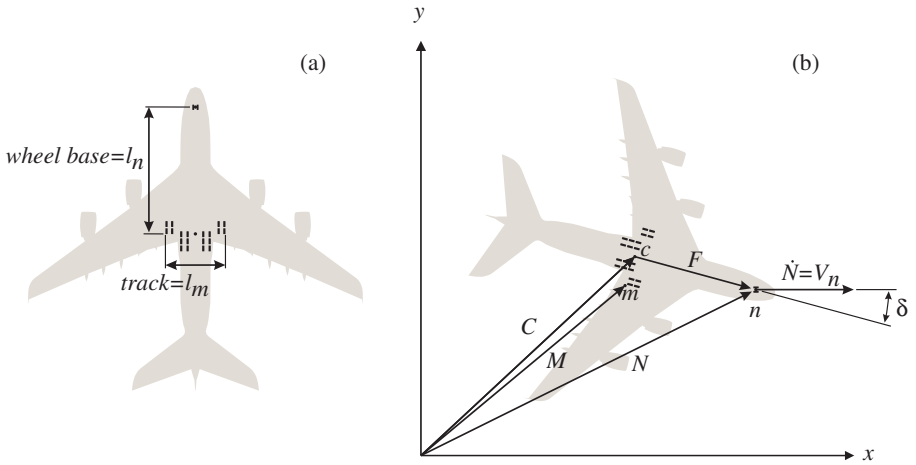

Figure 5: Aircraft representation with, (a) definition of the wheelbase and track width, (b) nose landing gear constraint in the form of a defined velocity vector V_n.

Note the units that are used. The velocity can be obtained by multiplying with the wheelbase. When written in the Cartesian coordinates that are normalised to the wheelbase, where $N = (n_x, n_y)$ and $C = (c_x, c_y)$, equation (1) becomes

$$\dot{c_x} = {n_x}^2\dot{n}_x - 2n_x\dot{n}_x c_x + n_x n_y \dot{n}_y - n_x \dot{n}_y c_y + \dot{n}_x {c_x}^2 - n_y \dot{n}_y c_x + \dot{n}_y c_x c_y \quad (1/\mathrm{s}), \tag{2}$$

$$\dot{c_y} = n_x \dot{n}_x n_y - \dot{n}_x n_y c_x + \dot{n}_y {n_y}^2 - 2n_y \dot{n}_y c_y - n_x \dot{n}_x c_y + \dot{n}_x c_x c_y + \dot{n}_y {c_y}^2 \quad (1/\mathrm{s}). \tag{3}$$

The steering angle δ is defined as the angle between the longitudinal axis of the aircraft and the longitudinal axis of the tug, and is given by

$$\delta = \cos^{-1}\left(\frac{\dot{N}\cdot(N-C)}{|\dot{N}|}\right). \tag{4}$$

A steering angle of zero indicates that the nose gear axle is perpendicular to the longitudinal axes of the aircraft. Kinematic simulations can provide some useful information for symmetric manoeuvres, but are not very useful when one considers asymmetric manoeuvres such as the U-turn [3].

III.B. Quasi-Steady Dynamics from Continuation Methods

The high cost associated with simulations makes continuation techniques attractive, due to the speed with which a global picture of the dynamics can be constructed [9]. Specific regions of interest can be identified for further detailed analysis with multibody dynamic codes [3]. A previous study of U-turn manoeuvres [3] described some of the theory behind bifurcation and continuation methods, and also showed how aircraft models are used in conjunction with the Dynamical Systems Toolbox that was developed within the MATLAB environment at the University of Bristol. The analysis starts by finding an equilibrium solution for the aircraft, either by simulation, or by a trimming routine. In our case, a velocity controller is used to control the engine thrust until a target velocity is reached. At this stage the steering angle is set to 0°. A continuation run is initiated as soon as the software recognises that an equilibrium condition has been reached (zero gradients for the continuation states). The algorithm then follows these equilibrium states as a parameter varies, while their stability is monitored. The presence of fold and Hopf bifurcations [10] (where the stability of the equilibrium solution is lost) is monitored as the steering angle is varied. In the applications in this paper we do not find any bifurcations. We do however use continuation algorithms in section IV to obtain steady-state turn-radii as the steering angle is varied. The steering angle that corresponds to the exit radius under consideration can then be obtained directly from this analysis, instead of using simulations.

III.C. Dynamic Methods

Many software packages use Lagrangian dynamics as a basis for developing computational algorithms for the dynamic analysis of multibody systems [11], where the final set of equations consists of differential and algebraic equations of index 3, which are considered to be of high complexity and, as a result, costly to solve [12]. This is the reason why multibody calculations tend to be difficult, and why alternative methods are useful. A comparison of the equations of motion for rigid bodies, when derived from Newtonian- and Lagrangian mechanics, leads to the same set of equations. However, the Lagrangian form does allow for the analysis of flexible bodies, leading to simulations that are even more computationally intensive when structural modes are included into the model. A detailed description of the calculations that are involved in multibody dynamics is not within the scope of this paper; the interested reader can obtain more details from references [11] and [13].

Multibody dynamics software is a key-enabler for aircraft ground performance predictions; figure 6 contains a schematic of typical components within an aircraft ground manoeuvrability model, in our specific case an A380 model. Figure 7 depicts a typical model for the nose landing gear. The first step of the modelling is to describe the rigid parts and the joints connecting the parts [13], where a part is described by its mass, inertia and orientation. The nose gear is constrained by a cylindrical joint between the main fitting and the strut, which is driven by an angular motion. Rotational joints are used for the steering system on the aft axles of the body landing gears, where the angles on the aft axles are controlled in response to the steering angle on the nose gear. Once the parts are defined, the next step is the addition of internal force elements to represent the shock absorbers and tyre forces, which are known as line-of-sight forces and which act between two parts. The vertical tyre force is modelled with an impact function that switches on as soon as the distance between the wheel centre and the tyre becomes less than the wheel radius. Lateral and torsional forces are implemented at the interface between the tyre and the ground, and are based on test data [14, 15]. Figure 7 depicts the components that are used for the nose gear, and similar elements are used for the other gears. External forces such as thrust and aerodynamic loads are added, and are known as action-only forces. The thrust can either be set to a constant value, or it can vary to maintain a specific velocity profile at either the CG or the nose of the aircraft. All geometric aspects are parameterised, from the axle-widths, wheel dimensions, gear positions, to the rake angles on the gears. This allows for great flexibility in terms of the analysis. See references [3] and [16] for further details on how the models are constructed.

IV. Steering Inputs

Previous studies of the steering angle variation during a turn have assumed a ramp function for the steering input [6]. In contrast, the International Civil Aviation Organization (ICAO) have derived exact solutions for the variation of the steering angle [17] based on kinematic equations, where they show that the steering angle variation is closer to an exponential function. We suggest that these equations are still too complex for everyday use by design engineers, and consequently empirical formulas that are easy to use are derived from kinematic simulations. Steering angles are also provided by the dynamic simulations as described in section III.C. The following section compares the steering angle variation that can be obtained from kinematic simulations, empirical estimates based on the kinematic simulations, bifurcation methods, as well as dynamic simulations. The steering angle variation consists of two distinct phases: the phase up to the exit point of the turn, and the phase where the aircraft straightens out.

IV..1. Steering Angle Variation During Circular Section of Exit

Equations (2) and (3) can be used to determine the trajectories by constraining the nose gear to the runway and taxiway centreline. The velocity vector is tangent to the circular trajectory for the duration of the turn. The analytical solution for the steering angle is given in reference [17] as

$$\delta = 2\tan^{-1}\left(\frac{1-e^{K\theta_n}}{R_n - K - R_n e^{K\theta_n} - Ke^{K\theta_n}}\right), \tag{5}$$

where the radius of turn is normalised to the wheelbase $R_n = \frac{r_n}{l_n}$, $K = \sqrt{R_n^2 - 1}$. The nose gear position in the turn is denoted by θ_n and is measured in radian, where the nose gear position is $\theta_n = 0^\circ$ at the start of the turn, and $\theta_n = 90^\circ$ at the exit of the turn. The final steady-state steering angle is derived in [4] as

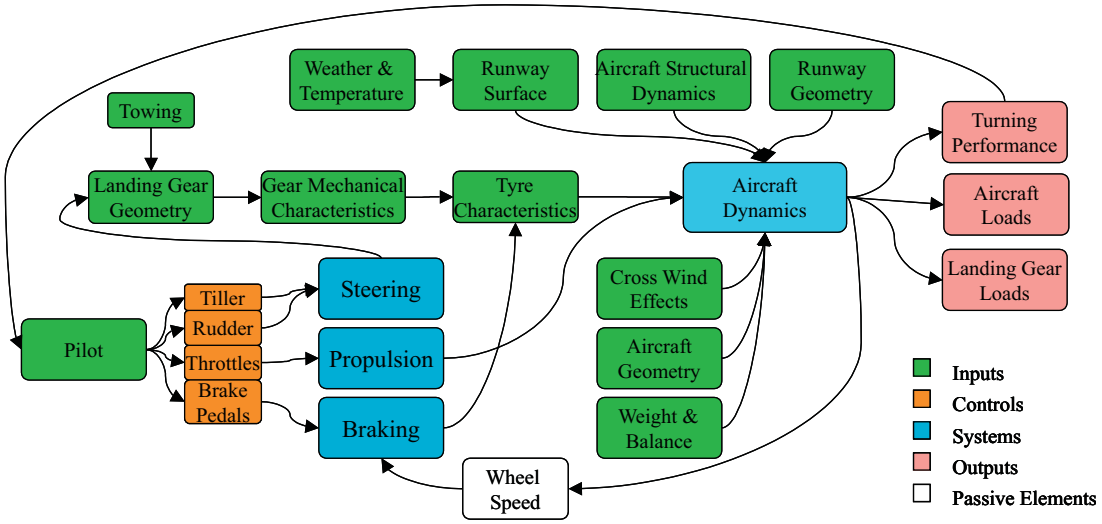

Figure 6: Ground manoeuvrability model components.

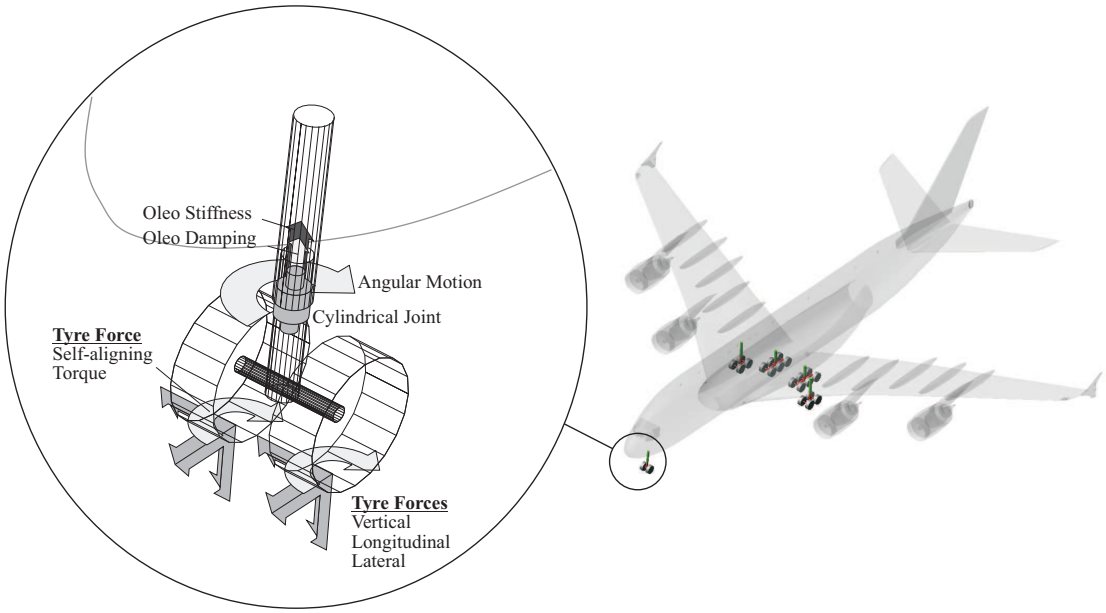

Figure 7: Detailed definition of nose gear components pertaining to an A380 model.

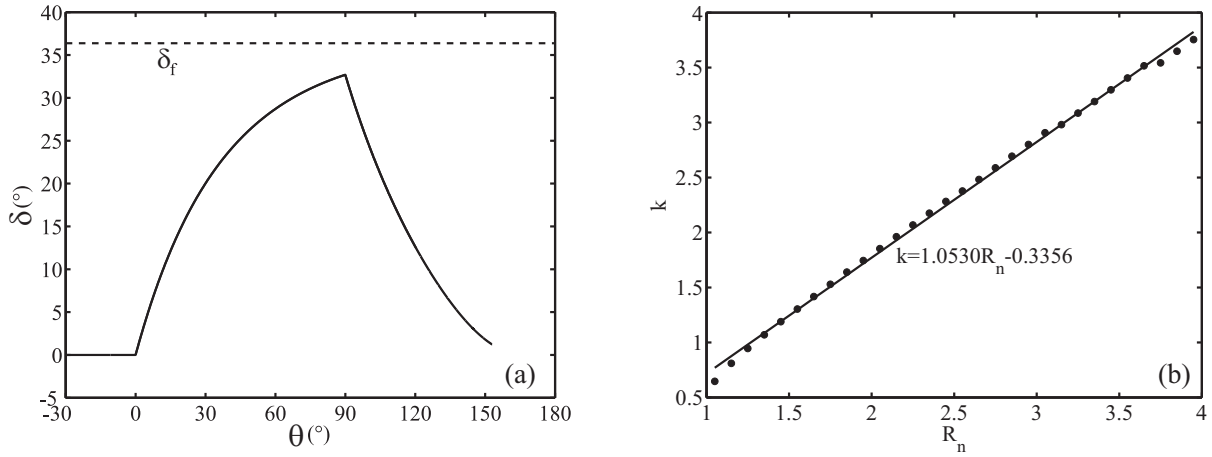

Figure 8: Steering angle input for a 90° turn; (a) depicts the steering angle variation during a 90° turn, while (b) gives an approximation for the fitted exponent in equation (8). Data points extracted from the simulations are indicated with dots.

$$\delta_f = \cos^{-1}\left(\frac{\sqrt{R_n^2 - 1)}}{R_n}\right). \tag{6}$$

A simpler formula that captures the steering angle variation δ during the turn, especially the maximum steering angle δ_{max}, is desirable, and consequently it was decided to obtain an empirical formula based on the results from the kinematic simulations in section V. Figure 8(a) contains the steering angle results for an exit manoeuvre that was obtained from simulating equation (1); it was concluded that the steering angle could be described by an equation of the form

$$\delta = \delta_f \left(1 - e^{-k\theta_n}\right). \tag{7}$$

Simulations were conducted for $R_n \in [1, 4]$, from which the steering angle for all the different combinations were extracted. Note that the normalised track width L_m is not important for the steering angle predictions. The steering angle builds up in an exponential way, where the exponent is dependent on the radius of turn r_n and the wheelbase l_n. The radius of turn is once again normalised to the wheelbase. It is therefore possible to find the appropriate exponent k by means of curve fitting methods. Figure 8(b) shows dots that represent individual exponents that were obtained in this way. A linear approximation can then be used to obtain the relationship between k and R_n and, therefore, the steering input required for a 90° runway exit is found as

$$\delta = \delta_f \left(1 - e^{-(1.053R_n - 0.336)\theta_n}\right). \tag{8}$$

Note that θ_n is defined in radians; if θ_n is converted to degrees, the equation becomes

$$\delta = \delta_f \left(1 - e^{-(0.018R_n - 0.006)\theta_n}\right). \tag{9}$$

Equations (8) and (9) are applicable to any exit, and consequently the angle that the taxiway makes with the runway can be inserted. The steering angle at the exit position would converge towards the steady-state steering angle as the exit radius is increased, or as the wheelbase is decreased; the latter can be seen clearly in figures 9(a) and 9(b). These graphs can also be used to estimate the steering angle requirements for other aircraft. Appendix A contains steering angle calculations for different aircraft types. The position of the nose gear on the circular trajectory can also be converted to the time domain to yield

$$\delta = \delta_f \left(1 - e^{-(1.053R_n - 0.336)\frac{V_n}{R_n}t}\right). \tag{10}$$

The velocity is normalised to the wheelbase and is expressed as wheelbase lengths per second. It is assumed that the velocity during the turn stays constant, which is not a realistic scenario for a constant

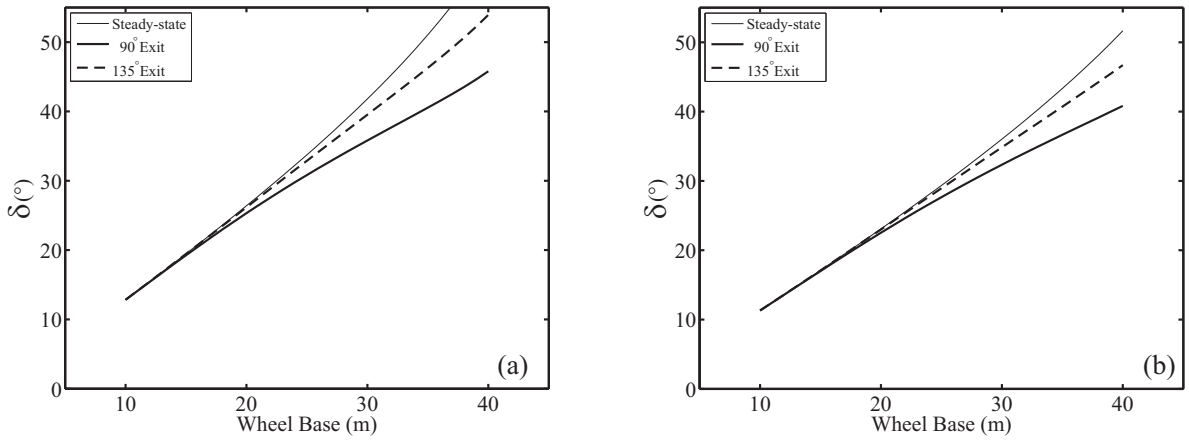

Figure 9: Maximum steering angle inputs for (a) Category V and (b) Category VI airports.

thrust configuration, as the velocity will decrease as the turn progresses [6]. The steady-state velocity for a specific steering angle can be obtained from a bifurcation diagram, and consequently an average velocity can be derived for equation (10). From simple geometry in figure 4, it can easily be shown that the heading angle ψ is the difference between the angular position of the nose gear on the circular trajectory, θ_n, and the steering angle δ. At the exit from the turn where $\theta_n = 90°$, the heading angle becomes

$$\psi_{90} = 90° - \delta \quad \text{deg.} \tag{11}$$

IV.A. Steering Angle Variation on Horizontal Section of Exit

The change in steering angle when the aircraft nose gear is moving on a horizontal line (x-direction) forms a tractrix [17] and can be derived from the y-coordinate of the main gear reference position c_y, which is calculated as [4]

$$c_y(t) = \frac{(k-1)\sin(\psi_{90} + 180°)}{ke^t - e^{-t}}. \tag{12}$$

The next step is to apply the initial conditions at the exit, thus when $\theta_n = 90°$. Set $t = 0$, and insert the heading angle from equation (11) at the exit ψ_{90}. The factor k is derived as

$$k = \frac{\cos(\psi_{90}) - 1}{\cos(\psi_{90}) + 1}. \tag{13}$$

The steering angle can then be calculated as

$$\delta(t) = \sin^{-1}(c_y(t)). \tag{14}$$

Design engineers are more interested in the maximum steering angle and the steering rate, hence, the need for a simplified equation in the previous section. No attempt will be made to derive a simpler equation describing the decrease in steering angle from the exit, as this is not a critical part of the manoeuvre.

IV.B. Steering Angle Predictions from Continuation Methods

The previous empirical and kinematic methods are adequate for calculating the towing angles during the preliminary and detail design phases. The steering angle predictions are similar to the towing predictions during the preliminary design phase, but do need to be refined for the detail design phase. Section IV..1 showed that a turn manoeuvre consists of a transition between a straight line and a circular manoeuvre, and

that the steady-state solution of the steering angle can be used in equation (8). This steady-state steering angle is however based on geometric methods, which ignore the tyre and aircraft dynamics.

Bifurcation methods, and more specifically, continuation methods, can provide the steady-state steering angle for different aircraft configurations, meaning that the tyre properties are taken into consideration [3]. The question is whether continuation methods provide a more accurate estimate of the steering profile compared to geometric methods. If so, the accuracy of the steering angle prediction can be improved at a smaller computational cost, compared to full dynamic simulations. A previous study related to U-turn manoeuvres [3] showed how a SimMechanics model of the A380 can be used with the Dynamical Systems Toolbox for the prediction of turn-widths. The same method is used here for the prediction of steering angles.

The turn radius can be calculated by dividing the velocity at the nose gear by the yaw rate; both these states are provided by the continuation analysis. Figure 10(a) shows the variation of the turn radius as the steering angle is increased for a velocity of 3 m/s. The steady-state steering angle that will provide a turn radius of 51 meters for Group VI airport taxiway turns can be read off the graph. In this case a steering angle of 37.9° will provide the required turn radius.

IV.C. Steering Angle Comparisons for the Different Methods

The pilot will usually try to maintain momentum (hence velocity) during the turn, by adjusting the thrust. Future automated systems are also likely to maintain a specific velocity profile during a turn, of which a constant velocity could be one of the candidates. A constant velocity controller, along with a controller to follow the centreline, was incorporated into the detailed dynamic model, allowing for a direct comparison of the steering angle for the different methods. Figure 10(b) contains a comparison of the input required from (i) a dynamic simulation, (ii) a kinematic simulation, (iii) an empirical solution (equations (10) and (14)), and (iv) a combination of the steady-state steering angle obtained from bifurcation methods with the empirical solution.

It can be observed from figure 10(b) that there is very good agreement between the empirical and the kinematic methods. An aircraft that is being propelled by its engines does however need a side-force on the nose gear, which is generated by a slip-angle. Typical slip-angle values for the nose gear during the turn would be between 2 and 3 degrees. The steering angle that is needed for the self-propelled case can either be provided by bifurcation methods or by simulations. We adapt the empirical method to include the self-propelled case, by using the steady-state steering angle that is provided from bifurcation methods in section IV.B, where we see that the steering angle predictions from the continuation method are close to the results from the simulations.

We can conclude that the empirical method is an adequate tool for the prediction of towing angles, due to the fact that the constraint forces are generated by the tug, and would be sufficient during the preliminary design phase. Bifurcation methods can be used in conjunction with empirical methods for the prediction of steering angles of an aircraft that is self-propelled, where a slip-angle on the nose gear is needed. Bifurcation methods would be adequate during the detailed design phase of a project.

V. Clearance Distances

Runway design rules published by the Federal Aviation Administration (FAA) use the steady-state trajectory to design the fillet sizes for a specific aircraft [18], while ICAO shows that the trajectory during the turn can be calculated from an elliptic integral [17], which can be evaluated with great effort. An equation for the deviation of the main gear centre position from the circular arc, which is dependent on the steering angle, is also derived in [17]. This is once again a difficult equation for design engineers to use, and it does not include the clearance distance of the inner gear reference position. It would therefore be useful to provide design rules on how the wheelbase and track width influence the performance characteristics. Figures 4(a) and (b) show the dimensions that are relevant to exit manoeuvres, where the dashed circle in figure 4(b) depicts the clearance distances for the inner gear, representing a worst case scenario; this is equivalent to the method used for predicting clearance distances by the FAA. Figure 4(b) also shows that the aircraft does not reach a steady-state, because the trajectory of the inner-gear reference position does not converge onto the dashed line that represents the steady-state for this reference position. More accurate estimates are needed to allow the design engineer more leeway with regard to the positioning of the gears.

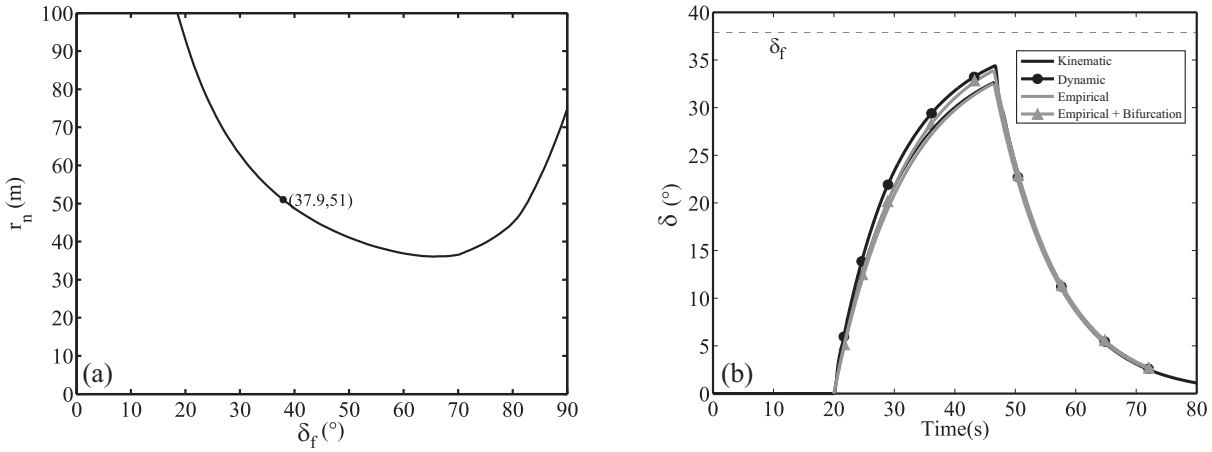

Figure 10: Steering angle comparisons; (a) steering angle obtained from continuation methods at a velocity of 3 m/s; (b) comparison of steering angle variation obtained from kinematic, dynamic, empirical and continuation (bifurcation) methods.

Simulations of the kinematic equations are used to obtain minimum clearance distances for varying wheelbase and track-width combinations. The radius of turn and the track width are normalised to the wheelbase, where $R_n \in [1, 4]$ and $L_m \in [0, 0.6]$. Here the only restriction is that the turn radius should not be smaller than the wheelbase, which is a reasonable assumption based on the aircraft and airport data that is available. The distance of the inner-gear reference position M from the centre of the turn is denoted by R_m, and it is monitored during the simulation. The angular position of point M relative to the negative x-axis is denoted by θ_m. The polar coordinates of the minimum clearance position can then be extracted from the calculations, and are denoted by $(R_{m90_{min}}, \theta_{m90_{min}})$. The dots in figure 11 are data points that are obtained from the kinematic simulations; they indicate the angular positions for a 90°- and a 135°-exit. The solid curves are fitted to the data points, where the angle of the inner gear reference position, at minimum clearance, for a 90°-exit is represented by

$$\theta_{m90_{min}} = -0.602{R_n}^2 + 7.378R_n + 56.526 \quad \text{(deg)}, \tag{15}$$

while the angular position of the inner gear reference position, at minimum clearance, for a 135°-exit is given by

$$\theta_{m135_{min}} = -1.580{R_n}^2 + 14.964R_n + 85.874 \quad \text{(deg)}. \tag{16}$$

The next step is to obtain an expression for the minimum clearance distance, for the inner gear reference position (normalised to the wheelbase) for a 90°-exit. An expression for the clearance distance can be obtained in a similar way as the method that was used for the steering angles. A surface can be fitted through the data (not shown), which can be described as

$$R_{m90min} = -0.024{R_n}^2 + 1.203R_n - 0.5L_m - 0.553. \tag{17}$$

An analysis of the results for a 135°-exit indicates that the minimum clearance distance for this turn can be described as

$$R_{m_{135min}} = -0.043{R_n}^2 + 1.323R_n - 0.5L_m - 0.742. \tag{18}$$

Note that the results are applicable to any aircraft; the A380 is used here as a case study to verify the results. Table 2 and figure 12 contain a comparison of the location of the minimum radial clearance of the inner gear reference position for a 90°-exit. It compares the values obtained from (i) a full dynamic simulation, (ii) a kinematic simulation, (iii) the empirical method that was derived in equations (15) and (17), and (iv) the steady-state position that is used for airport planning purposes by the FAA [18]. A simple controller was designed for the dynamic simulation, where any point can be set to follow the centreline, with the nose gear defined as the reference point for this specific study. The pilot is assumed to act as a closed

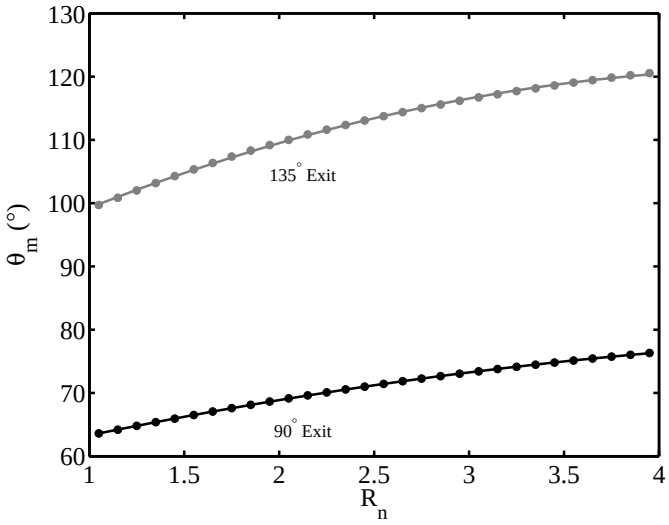

Figure 11: Angular position where minimum radius occurs for inner gear reference position; Dots indicate data points obtained from simulations, and the solid curve is fitted.

Table 2: Minimum clearance location of inner gear reference position when the COC method is used for a 90°-exit.

	Number	X coordinate (m)	Y coordinate (m)	Distance from origin (m)	Distance rel. to 1 (m)	Distance Error (%)
Dynamic	(i)	−13.76	33.08	35.83	0.00	0.00
Kinematic	(ii)	−13.62	32.74	35.46	0.37	1.04
Empirical	(iii)	−13.67	32.61	35.36	0.48	1.34
steady-state	(iv)	−20.10	27.29	33.89	8.58	23.96

loop controller with the aim of keeping the area around the cockpit above the centreline. The errors from the kinematic and empirical methods are calculated as

$$e = 1 - \frac{M_{1_{min}} - M_{j_{min}}}{|M_{1_{min}}|}. \tag{19}$$

Following the convention in figure 5, where M is the position vector of the inner-gear reference position, $M_{1_{min}}$ denotes the minimum radius vector position for the dynamic simulation case. The other positions are denoted by $M_{j_{min}}$ where j represents the label of the case under consideration. The results from the empirical predictions are within 1.5% of the results from the dynamic simulations. It can be concluded from figure 12 that equation (17) gives a good estimate of the clearance distance that can be achieved for a 90°-exit; in particular, the estimate is significantly better than the steady-state approximation. The same holds true for the 135° case, although the minimum radial distance is close to the steady-state value.

Feasible wheelbase and track width combinations can be determined by inserting a minimum radial distance into equations (17) and (18), and then recasting the equations so that the track width appears on the left-hand side. The fillet radius for Group V and VI airports is assumed to be 25.9 meters [7], where a minimum clearance distance of 4.5 meters is needed [17]. The locus of track widths that provide a radius of 30.4 meters will therefore provide the boundary for the feasible region of wheelbase and track widths.

Figure 13 depicts such an envelope for the different types of airports and exits. The area to the right of a hatched line indicates a clearance distance of less than 4.5 meters for the particular case. The wheelbase that is depicted on the x-axis, could also be replaced by the distance from the cockpit to the main gear reference position, which would represent the COC method. We have assumed that the nose gear will follow

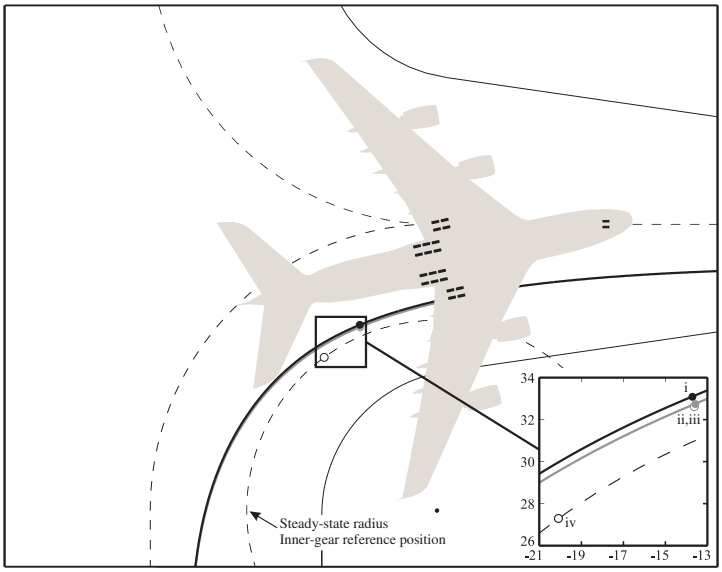

Figure 12: Minimum clearance location of inner gear reference position for a 90° exit, COC method for different calculation techniques: (i) dynamic , (ii) kinematic , (iii) empirical, (iv) steady-state, based on the FAA method.

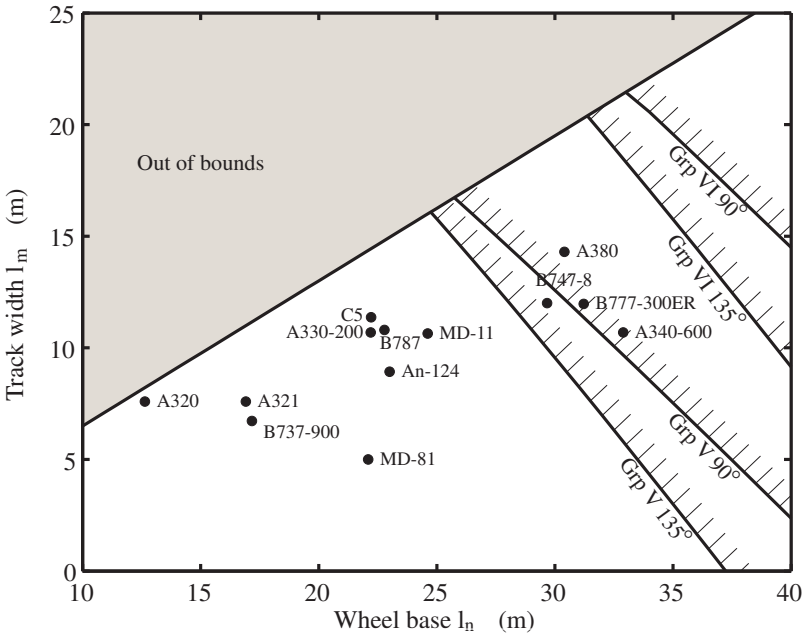

Figure 13: Envelopes for Group V and VI runway exits with data points for selected aircraft, where the COC method is employed.

the centreline. It is possible to overlay the data for any aircraft onto the graph, making the method useful for comparative purposes. We have overlaid the data in Appendix A, where it can be seen that the COC minimum clearance distance for the A380 lies to the right of the required margins for Group V airports, hence the JOS method needs to be employed for this type of airport; this is consistent with the Airplane Characteristics Manual for the A380 [7]. Note the prediction for the B747-8, for which it is predicted that the aircraft will have sufficient clearance on a Group V airport with a 90° exit, but not for a 135° exit. It can be concluded that figure 13 can be used as a useful design tool at the early stages of an aircraft programme. On the other hand, the final clearance distances that are published in the Aircraft Characteristics Manual should still be obtained from detailed dynamic simulations.

VI. Conclusions

Steering angle and clearance distance predictions for runway exits manoeuvres are of great value during the preliminary design phase of an aircraft programme, but these predictions are usually hampered by a lack of data for detailed simulation models at such an early stage. The challenges related to multibody dynamic simulations have been discussed, especially the difficulty of building detailed models, as well as the computational challenges surrounding the integration of the equations of motion. Alternative methods were presented to obtain such predictions, where we focussed on empirical methods, kinematic methods, and bifurcation methods, more specifically, continuation methods. Comparisons were made between these methods and a detailed simulation model, showing very good agreement.

An empirical formula was derived from kinematic equations that are used for towing, to evaluate the steering angle variation during a 90°-exit manoeuvre. This empirical formula showed very good agreement with kinematic and dynamic simulations. A steering input was derived from a dynamic model with a controller for additional validation purposes, where the controller is used to maintain the nose landing gear on the taxiway line. The steering angle obtained with the controller showed only small differences from the steering angle obtained from the kinematic method, due to a slip-angle that is needed when the dynamic method is used. This slip-angle is responsible for the generation of a side force that maintains the circular trajectory of the nose landing gear. More accurate predictions of the final steering angle can be obtained by using continuation methods, which are in close agreement with the values obtained from simulations. The advantage of the continuation approach, compared to simulations, is that it is more efficient in terms of run-times and can be used to generate steady-state information.

We also used the kinematic equations for the prediction of clearance distances for runway exits. The equations are normalised to the wheelbase and are therefore valid for any track width and wheelbase combination. The only restriction is that the turn radius should not be smaller than the wheelbase, which is a reasonable assumption based on the aircraft and airport data that is available. A comparison of clearance distances was made between a validated dynamic model, a kinematic model, an empirical model that is derived from the kinematic model, and a geometric method used by the FAA. It was shown that the clearance distances for the kinematic and empirical methods are within 1.5% of the predicted clearance distance that is obtained from the dynamic model. The geometric method is a worst-case scenario that is useful for airport planning purposes, but not for aircraft design. The empirical model, on the other hand, can be used as a useful tool by design engineers for the prediction of clearance distances of any type of exit or aircraft configuration.

References

[1] Airbus Operations, "Airbus MoU with IAI to explore eco-efficient "engines-off" taxiing," http://www.airbus.com/en/presscentre/pressreleases/pressreleases_items/09_06_17_eco_efficient_taxiing.html, [retrieved 25 March 2010].

[2] Advisory Council for Aeronautics Research in Europe, "2008 Addendum to the Strategic Research Agenda," http://www.acare4europe.com/docs/ACARE_2008_Addendum.pdf, [retrieved 15 October 2009].

[3] Coetzee, E., Krauskopf, B., and Lowenberg, M., "Application of Bifurcation Methods to the Prediction of Low-Speed Aircraft Ground Performance," *Accepted for publication - Journal of Aircraft*, 2010.

[4] Fossum, T. and Lewis, G., "A mathematical model for trailer-truck jackknifing," *SIAM Review*, Vol. 23, No. 1, 1981, pp. 95–99.

[5] Coetzee, E., *Nonlinear aircraft ground dynamics*, Master's thesis, University of Bristol, 2006.

[6] Rankin, A., Krauskopf, B., Lowenberg, M., and Coetzee, E., "Nonlinear analysis of lateral loading during taxiway turns," *Accepted for publication - Journal of Aircraft*, 2010.

[7] Airbus Operations, "A380 Airplane Characteristics Manual,"

http://www.airbus.com/fileadmin/media_gallery/files/tech_data/AC/AC_A380oct09.pdf, [retrieved 15 October 2009].

[8] De Falco, D., Pennestrì, E., and Vita, L., "The Udwadia-Kalaba formulation: A report on its numerical efficiency in multibody dynamics simulations and on its teaching effectiveness," *Multibody Dynamics*, 2005, pp. 21–24.

[9] Krauskopf, B., Osinga, H. M., and Galán-Vioque, J., *Numerical Continuation Methods for Dynamical Systems*, Springer, 2007.

[10] Kuznetsov, Y., *Elements of Applied Bifurcation Theory, Applied Mathematical Sciences, Vol. 112*, Springer-Verlag, September 1998.

[11] Shabana, A., *Dynamics of Multibody Systems*, Cambridge University Press, 2nd ed., October 2003.

[12] Negrut, D. and Harris, B., "ADAMS theory in a nutshell," http://www.mscsoftware.com/, [retrieved 04 February 2008].

[13] Blundell, M. and Harty, D., *The Multibody Systems Approach to Vehicle Dynamics*, SAE, September 2004.

[14] Thota, P., Krauskopf, B., and Lowenberg, M., "Shimmy in a nonlinear model of an aircraft nose landing gear with non-zero rake angle," *AIAA Modeling and Simulation Technologies Conference*, , No. AIAA-2008-6529, August 2008.

[15] Thota, P., Krauskopf, B., and Lowenberg, M., "Interaction of torsion and lateral bending in aircraft nose landing gear shimmy," *Nonlinear Dynamics*, Vol. 57, No. 3, 2009, pp. 455–467.

[16] Rankin, J., Coetzee, E., Krauskopf, B., and Lowenberg, M., "Bifurcation and Stability Analysis of Aircraft Turning on the Ground," *Journal of Guidance, Control, and Dynamics*, Vol. 32, no. 2, No. 0731-5090, April 2009, pp. 500–511.

[17] International Civil Aviation Organization, "Aerodrome Design Manual (Doc 9157) Part 2: Taxiways, Aprons and Holding Bays," Tech. Rep. 9157,AN/901, 2005.

[18] Federal Aviation Administration, "Advisory Circular, Airport Design," Tech. Rep. 150/5300-13, 1989.

[19] Airbus Operations, "Aircraft Characteristics,"
http://www.airbus.com/en/services/customer-services/maintenance-engineering/tech-data/aircraft-characteristics/, [retrieved 15 October 2009].

[20] Boeing, "Commercial Airplanes," http://www.boeing.com/commercial/, [retrieved 15 October 2009].

[21] Anon., "Antonov Basic Technical Data," http://www.aviastar-sp.ru/aviastar_en/aircraft/an124/an124.htm, [retrieved 24 June 2010].

[22] Anon., "Lockheed C-5 Galaxy," http://www.militaryaviation.eu/transporter/Lockheed/C-5.htm, [retrieved 24 June 2010].

[23] Gomes de Barros, A. and Chandana Wirasinghe, S., "New aircraft characteristics related to airport planning," www.ucalgary.ca/EN/Civil/NLAircraft/Atrgpap.pdf, [retrieved 1 May 2010].

VII. Appendix A

The wheelbase and track width data in table 3 were obtained from references [19], [20], [21], [22] and [23]. Table 4 contains the calculated steering angles that are achieved for different aircraft types, based on the equations in section IV. Tables 5 and 6 contain estimates for the minimum radial location of the inner gear reference position, from the origin of the centreline, based on the equations in section V.

Table 3: Aircraft dimensions

AC Type	Wheelbase l_n (m)	Track Width l_m (m)	L_m
A320	12.64	7.59	0.60
A321	16.91	7.59	0.45
A330-200	22.20	10.69	0.48
A340-600	32.89	10.69	0.33
A380	30.40	14.30	0.47
An-124	23.00	9.00	0.39
C5	22.22	11.42	0.51
B737-900	17.17	6.72	0.39
B747-8	29.67	12.00	0.40
B777-300ER	31.22	11.97	0.38
B787	22.78	10.80	0.47
MD-81	22.10	5.10	0.23
MD-11	24.60	10.70	0.43

Table 4: Steering angles for Group V and VI Airports

AC Type	Grp V ($r_n = 45.7m$)				Grp VI ($r_n = 51.0m$)			
	R_n	δ_f	δ_{90}	δ_{135}	R_n	δ_f	δ_{90}	δ_{135}
A320	3.62	16.06	15.99	16.05	4.03	14.35	14.32	14.35
A321	2.70	21.72	21.30	21.66	3.02	19.36	19.14	19.34
A330-200	2.06	29.06	27.43	28.68	2.30	25.80	24.83	25.61
A340-600	1.39	46.03	38.20	42.80	1.55	40.16	34.92	38.27
A380	1.50	41.70	35.82	39.49	1.68	36.59	32.72	35.33
An-124	1.99	30.22	28.30	29.74	2.22	26.81	25.65	26.57
C5	2.06	29.09	27.45	28.70	2.30	25.83	24.85	25.64
B737-900	2.66	22.07	21.61	22.00	2.97	19.67	19.43	19.65
B747-8	1.54	40.48	35.12	38.53	1.72	35.57	32.06	34.47
B777-300ER	1.46	43.09	36.61	40.58	1.63	37.75	33.46	36.30
B787	2.01	29.90	28.06	29.44	2.24	26.53	25.42	26.30
MD-81	2.07	28.92	27.32	28.54	2.31	25.68	24.72	25.49
MD-11	1.86	32.57	30.01	31.85	2.07	28.84	27.26	28.47

Table 5: Minimum clearance location of inner-gear reference position at Group V airports.

AC Type	$\theta_{m_{90_{min}}}$ (◦)	$r_{m_{90_{min}}}$ (m)	$\theta_{m_{135_{min}}}$ (◦)	$r_{m_{135_{min}}}$ (m)
A320	75.33	40.16	119.33	40.12
A321	72.07	38.82	114.78	38.76
A330-200	69.16	35.06	109.99	34.56
A340-600	65.61	29.89	103.62	27.96
A380	66.26	29.34	104.80	27.77
An-124	68.81	35.54	109.37	34.95
C5	69.15	34.69	109.97	34.18
B737-900	71.90	39.15	114.52	39.08
B747-8	66.46	30.85	105.18	29.39
B777-300ER	66.04	30.10	104.40	28.41
B787	68.90	34.74	109.54	34.18
MD-81	69.21	37.90	110.07	37.41
MD-11	68.15	33.95	108.22	33.17

Table 6: Minimum clearance location of inner-gear reference position at Group VI airports.

AC Type	$\theta_{m_{90_{min}}}$ (◦)	$r_{m_{90_{min}}}$ (m)	$\theta_{m_{135_{min}}}$ (◦)	$r_{m_{135_{min}}}$ (m)
A320	76.50	45.55	120.54	45.37
A321	73.30	44.45	116.64	44.46
A330-200	70.30	40.87	111.92	40.57
A340-600	66.52	35.89	105.28	34.29
A380	67.21	35.30	106.53	34.05
An-124	69.93	41.37	111.29	41.00
C5	70.29	40.50	111.90	40.20
B737-900	73.13	44.80	116.39	44.80
B747-8	67.43	36.81	106.93	35.65
B777-300ER	66.97	36.07	106.11	34.71
B787	70.03	40.57	111.46	40.21
MD-81	70.35	43.71	112.00	43.42
MD-11	69.23	39.82	110.11	39.28